Organic Electronics 37 (2016) 47–54

Contents lists available at ScienceDirect

Organic Electronics

journal homepage: www.elsevier.com/locate/orgel

Potassium-neutralized perylene derivative (K_4PTC) and rGO-K_4PTC composite as effective and inexpensive electron transport layers for polymer solar cells

Zhenggen Gu [a, 1], Dongying Zhou [a, 1], Bingbing Sun [a], Mingliu Tang [a], Kai Chen [a], Lai Feng [a, *], Yi Zhou [b]

[a] College of Physics, Optoelectronics and Energy & Collaborative Innovation Center of Suzhou Nano Science and Technology, Soochow University, Suzhou 215006, China

[b] Laboratory of Advanced Optoelectronic Materials, College of Chemistry, Chemical Engineering and Materials Science, Soochow University, Suzhou 215163, China

ARTICLE INFO

Article history:
Received 21 April 2016
Received in revised form
7 June 2016
Accepted 7 June 2016

Keywords:
Polymer solar cells
Graphene
Electron transport layer
Degradation
Work function

ABSTRACT

The polymer solar cell (PSC) with Ca/Al electrode always suffers from low stability mainly due to the incorporation of oxygen and moisture-sensitive Ca electron-transport interlayer (ETL). To alleviate this problem, air-stable alternatives to Ca ETL are highly desired. Herein, we report two solution-processable, air-stable, effective and inexpensive ETLs based on potassium-neutralized perylene tetracarboxylic derivative (K_4PTC) and its rGO composite (rGO-K_4PTC), respectively. These ETL materials were facilely prepared and characterized by means of UV-vis, FL, FTIR, XPS and UPS. Importantly, both ETLs exhibited a low work function (WF) of 4.0 eV, which well matches the LUMO level of fullerene acceptors and allows their use as ETL in PSCs. As a result, the P3HT and PTB7-th-based devices with respective ETL remarkably outperformed those without ETL yielding increases of ~35% in power conversion efficiencies (PCEs), which indicates good electron-transporting capabilities of K_4PTC and rGO-K_4PTC interlayers. The high-performance PSCs with the ETL gave average PCEs of 6.17–6.18% (for PTB7-th:PC_{61}BM-based devices) and 7.26% (for PTB7-th:PC_{71}BM-based devices), respectively, fairly comparable to those of Ca/Al devices (6.50% and 7.50%). Furthermore, the rGO-K_4PTC device exhibited stability higher than that of the K_4PTC device probably due to the fact that the rGO-K_4PTC layer can provide more efficient protection for the active layer against degradation. Thus, rGO-K_4PTC layer might be more suitable for real applications as compared to the K_4PTC layer.

1. Introduction

Polymer solar cells (PSCs) have been of continuous interest in recent years because of their ease of fabrication, low cost, light weight and promising flexibility [1–4]. Very recently, both single-junction and tandem PSCs announced power-conversion efficiencies (PCEs) exceeding 10%, showing a promising potential for commercialization [5–7]. However, there are so far several drawback issues retarding the real applications of PSCs. For example, PSCs generally surfer from low stability, especially, in the presence of oxygen and humidity [8–11]. This might be attributed mainly to the use of moisture and oxygen-sensitive cathode such as Ca/Al. To overcome this drawback issue, one approach is to replace the active Ca interlayer by alternative materials, allowing not only the promotion of device stability but also the efficient electron transport from the active layer to the cathode.

Up to date, the state-of-art materials used for electron transport layer (ETL) include metal fluorides [12,13], n-type metal oxides [14–17] and n-type organic compounds [18–29]. All of them showed improved stabilities against oxygen and humidity. In particular, recent efforts have been devoted to developing various organic ETL materials which are solution processable and compatible with the high-throughput roll-to-roll process of PSCs. For example, the ETLs based on conjugated polyelectrolytes [18–20], perylene diimide derivatives [21], fullerene and graphene derivatives [22–29] displayed comparable or even better

* Corresponding author.
E-mail address: fenglai@suda.edu.cn (L. Feng).
[1] These authors contribute equally to this work.

http://dx.doi.org/10.1016/j.orgel.2016.06.013
1566-1199/

performance with respect to the conventional Ca interlayer. However, many of organic ETL materials require multi-step synthesis and purification. The high-cost production might limit their applications in cost-effective PSCs. This motivates us to search for low-cost but efficient organic ETL materials.

Herein, we first report the use of potassium-neutralized perylene tetracarboxylic derivative (K_4PTC) and its rGO composite (rGO-K_4PTC) as effective and low-cost interfacial ETLs. Importantly, both K_4PTC and rGO-K_4PTC exhibit low work functions (WF) of *ca.* 4.0 eV (*vide infra*), which well matches the LUMO of fullerene acceptor [29,30], in favor of the electron transport process. As a proof of concept, we applied these ETLs to various PSCs based on poly(3-hexylthiophene) (P3HT) and low bandgap polymer poly [(ethylhexyl-thiophenyl)-benzodithiophene-(ethylhexyl)-thienothiophene] (PTB7-th) [31], respectively. As compared to the reference device without ETL, the device with respective ETL gave remarkable PCE enhancements of ~35%. Moreover, rGO-K_4PTC ETL provides better device stability in air, thus suggesting its superiority relative to the K_4PTC ETL.

2. Experimental

2.1. Preparation of K_4PTC (potassium salt of perylene-3,4,9,10-tetracarboxylate)

K_4PTC was prepared according to the previously reported method [32]. In details, perylene *p*-dianhydride (5.0 g, 0.013 mol) was mixed with a 2 M aqueous KOH solution with a molar ratio of ca. 1:4.5. The resulting mixture was refluxed overnight, yielding a luminescent yellow solution. This solution was dropwise added to acetone to form yellow participate, which can be collected by centrifugation and washed by water/acetone mixture. Finally, the resulting yellow power was vacuum-dried at room temperature.

2.2. Preparation of the composite of rGO-K_4PTC

Graphene oxide (GO) was prepared using modified Hummers method [33]. To prepare rGO-K_4PTC composite, the as-prepared GO (5 mg) was dispersed in 10 mL water solution containing 7.5 mg K_4PTC by ultrasonication. The mixture was then stirred at 50–60 °C for 12 h, followed by adding $NaBH_4$ (6 mg) and refluxing for additional 3 h. Finally, the resulting solution was subjected to multiple centrifugations or dialysis for two days to remove inorganic salts and most unreacted K_4PTC from the composite of rGO-K_4PTC.

2.3. Characterizations

UV-Vis absorption and fluorescence spectra were obtained on a Shimazu UV2600 UV-vis spectrometer and a Hitachi F-4600 spectrophotometer, respectively. Micro-fourier transform infrared (FTIR) spectra were recorded on a Nicolet Magnaestimated-750 (fitted with a Nic-plan Microscope IR) spectrometer. Raman spectra were measured by an instrument of Horiba Jobin Yvon using an Ar^+ ion CW laser of 633 nm as an excitation source. X-ray diffraction (XRD) patterns were obtained on a Bede D1 X-ray diffractometer (UK, Bede Scientific Ltd.). X-ray photoelectron spectroscopy (XPS) studies were carried out with an ESCALAB 250 spectrometer using a monochromated Al Kα excitation source. The ultraviolet photoelectron spectroscopy (UPS) spectra were obtained on an AXIS Ultra-DLD using HeI irradiation with $h\nu = 21.23$ eV. Morphology of the active layers was studied using MFP-3D-BIO (Asylum Research) atomic force microscopy (AFM) in tapping mode. Scanning electron microscopy (SEM) images were obtained with a Hitachi SU8010 instrument.

2.4. Device fabrication and measurements

P3HT, PTB7-th and [6,6]-phenyl C_{61}-butyric acid methyl ester ($PC_{61}BM$), $PC_{71}BM$ were purchased from Solarmer Material Inc. The indium tin oxide (ITO) glass was cleaned through a multi-step ultrasonication process (in deionized water with detergent, acetone and isopropanol). The standard PSCs were fabricated with a configuration of the traditional sandwich structure (i.e., ITO/PEDOT:PSS/active layer/Ca/Al). Firstly, a thin layer (40 nm) of poly(3,4-ethylenedioxythiophene):poly(styrene sulfonate) (PEDOT:PSS) (Baytron PVP Al 4083 Germany) was spin-coated on an ITO glass, followed by baking at 150 °C for 30 min in air. Then, for common PSCs, the active layer was deposited on the top of the PEDOT:PSS layer by spin-coating a dichlorobenzene solution (*o*-DCB, 0.5 mL) containing a mixture of P3HT:$PC_{61}BM$ (10 mg:10 mg) at 800 rpm for 40 s. Next, a slow evaporation of active-film was carried out by keeping the film in a petri dish fill with a drop of *o*-DCB overnight, followed by thermal treatments (150 °C for 10 min). For high-performance PSCs, a *o*-DCB solution (1 mL) containing a mixture of PTB7-th:$PC_{61}BM$ (10 mg:15 mg) and 1,8-diiodooctance (3 vol %) was spin-cast on the prepared substrate at 1000 rpm for 90 s. Finally, a Ca/Al (20/80 nm) electrode was deposited on the active layer with a shadow mask *via* thermal evaporation under a vacuum of ca. 10^{-5} Pa. Alternatively, ETL with the thickness of ~5 nm was deposited on the active layer by spin coating a water/ethanol (1:4, v:v) solution containing K_4PTC or composite of rGO-K_4PTC (0.2 mg mL^{-1}) at 800 rpm for 60 s. Additional thermal annealing process at 80 °C for 1 min was performed for the P3HT-based system. The thicknesses of the ETLs were measured by a spectroscopic ellipsometry alpha-SE (J. A. Woollam CO., Inc., USA) and analyzed from the companying software Complete EASE 4.68 (J. A. Woollam CO., Inc., USA). The active area of the device was 4 mm^2. The current density–voltage (*J*–*V*) measurement of the device was performed with a Keithley 2400 SourceMeter under simulated Air Mass 1.5 Global (AM. 1.5 G) solar illumination with an intensity of 100 mW cm^{-2}. The light source was calibrated using a standard silicon solar cell before use. The incident photon-to-current conversion efficiency (IPCE) was measured by a solar cell spectral response measurement system QE-R3011 (Enli Technology Co., Ltd.). The light intensity was calibrated using a single-crystal silicon photovoltaic cell before measurement. The degradation tests were performed under moisture condition (ca. 60% relative humidity) without any encapsulation. The photovoltaic degradation performances of the 3 tested cells were averaged.

The electron-only devices were fabricated with a configuration of ITO/Cs_2CO_3/P3HT:$PC_{61}BM$/with or without ETL/Al. The Cs_2CO_3 layer (~10 nm) was firstly spin-coated on an ITO glass substrate. Then, an active layer (~150 nm), an ETL (~5 nm) and Al cathode (~100 nm) were deposited in sequence on the Cs_2CO_3 layer. *J*-*V* curves were measured in dark using Keithley 2400 SourceMeter.

3. Results and discussion

3.1. Preparations and characterizations

In a typical experiment, K_4PTC was readily synthesized via a simple hydrolysis reaction [32]. rGO was produced by reducing GO that was prepared using the modified Hummers method [33]. The rGO-K_4PTC composite (Scheme 1) was prepared via a non-covalent functionalization approach. The resulting K_4PTC and rGO-K_4PTC were characterized *via* a series of spectroscopic methods to confirm their compositions and to investigate their electrical natures.

Fig. 1a provides the UV-vis absorption spectra of K_4PTC and rGO-K_4PTC. Specifically, K_4PTC shows feature absorptions at 219, 261, 438 and 467 nm, in agreement with the previous reports [34]. rGO-

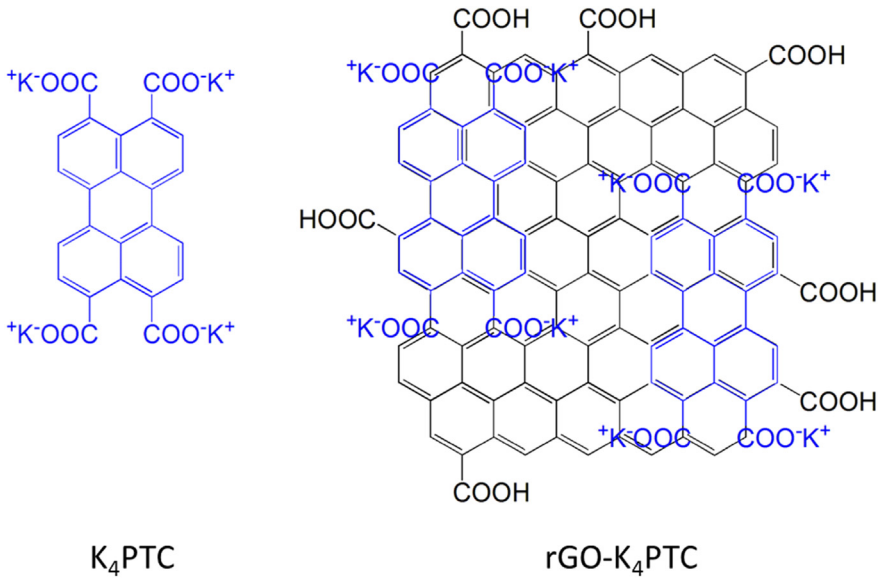

Scheme 1. Schematic structures of K_4PTC and $rGO\text{-}K_4PTC$.

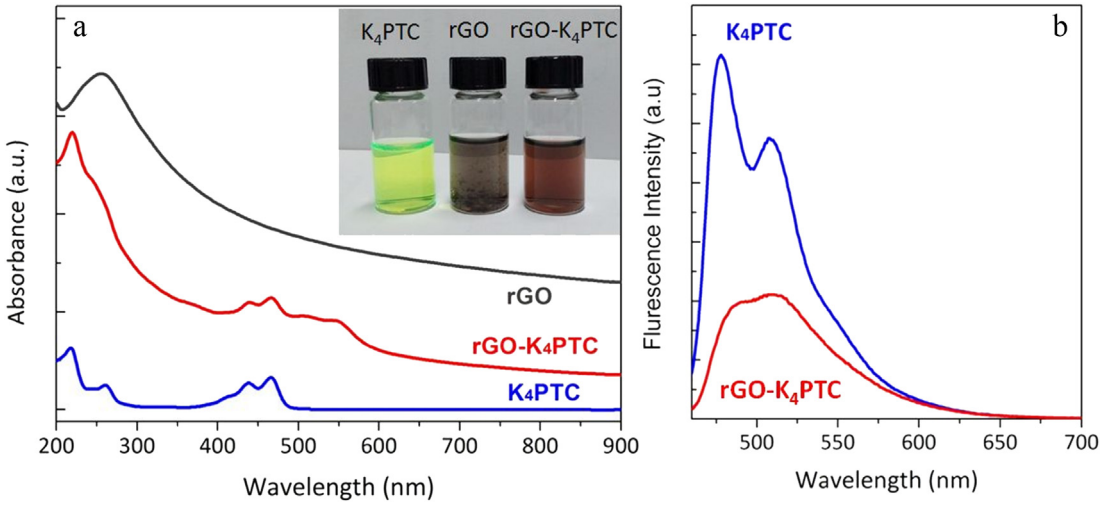

Fig. 1. (a) UV-vis absorption spectra of K_4PTC and $rGO\text{-}K_4PTC$ in comparison with rGO in water solution. The inset shows their photo. (b) Fluorescence spectra of K_4PTC and $rGO\text{-}K_4PTC$ in water solution, photoexcited at 438 nm after the absorption normalization at the excitation wavelength.

K_4PTC displays the characteristic absorption peak of rGO at 255 nm along with two broad absorptions at 518 and 548 nm, which can be attributed to the $0 \rightarrow 1$ and $0 \rightarrow 0$ transitions of the K_4PTC moieties that are noncovalently grafted with the rGO nanosheets. These absorptions are red shifted by 80 nm relative to those of the free or ungrafted K_4PTC moieties, implying the significant π-π stacking interactions between the K_4PTC moieties and rGO nanosheets [35]. Besides, additional absorptions at 438 and 467 nm were also observed for $rGO\text{-}K_4PTC$, suggesting the presence of residual ungrafed K_4PTC in the composite. The inset photography included in Fig. 1a presents a red-brown solution of $rGO\text{-}K_4PTC$, which is unlike the luminescent solution of K_4PTC as well as the deep gray solution of rGO, indicating the formation of new composite. The florescence assays (Fig. 1b) reveal a rather strong quenching of the K_4PTC florescence for the composite of $rGO\text{-}K_4PTC$, thus confirming the significant π-π interaction between the individual components. Raman spectroscopy was further used to probe the interaction between individual components of $rGO\text{-}K_4PTC$. As shown in Fig. S1, no evident shift can be observed in G and 2D bands (1589 cm^{-1} and 2650 cm^{-1}) of $rGO\text{-}K_4PTC$, as compared with those of rGO, indicating negligible charge-transfer between the rGO and grafted K_4PTC [36]. On the other hand, the samples of K_4PTC and $rGO\text{-}K_4PTC$ drop-casting on silicon wafer were investigated by scanning electron microscope (SEM). As shown in Fig. S2, fine powders are seen for K_4PTC, while multiple rGO nanosheets along with attached K_4PTC powders can be clearly detected in $rGO\text{-}K_4PTC$. This result thus directly demonstrates the hybrid nanostructure of the composite. Fig. S3 shows the XRD patterns of K_4PTC and $rGO\text{-}K_4PTC$. For $rGO\text{-}K_4PTC$, only a broad diffraction peak at ca. 24° corresponding to rGO can be clearly observed while the characteristic peaks of the crystalline K_4PTC disappear completely. This result might suggest that the K_4PTC molecules grafted on the rGO are random-oriented.

For insight into the surface chemical compositions of K_4PTC and $rGO\text{-}K_4PTC$, XPS analyses were conducted. In particular, K_4PTC and $rGO\text{-}K_4PTC$ present very similar XPS profiles (Fig. 2) which differ from that of rGO. Both spectra exhibit the signals corresponding to

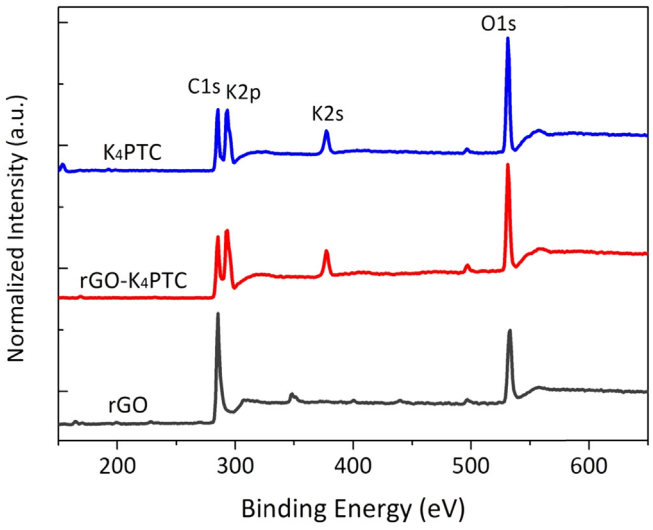

Fig. 2. XPS profiles of K_4PTC, rGO-K_4PTC and rGO.

C1s, O1s, K2s and K2p orbitals, in good agreement with the composition of K_4PTC. Nevertheless, the high-resolution C1s spectrum of rGO-K_4PTC is found to be slightly different from that of K_4PTC (see Fig. S4). The former spectrum can be well fitted by four peaks, corresponding to not only the K_4PTC carbons (in C=C and COO^-K^+ groups) but also the rGO-related carbons (in C-OH/C-O and COOH groups). In addition, by comparing the FT-IR spectra of rGO-K_4PTC and rGO (Fig. S5), one of common peaks was found at ~1200 cm^{-1}, corresponding to the C-O-C stretching vibrations, which is otherwise unseen in the spectrum of K_4PTC. Thus, the combined studies of XPS and FT-IR confirm the hybrid compositions of rGO-K_4PTC.

The work functions (WFs) of the K_4PTC and rGO-K_4PTC layers were determined by ultraviolet photoelectron spectroscopy (UPS). Fig. 3 illustrates their secondary electron cutoff spectra, in comparison with those of the rGO layer and ITO electrode. In particular, the WF of ITO was calculated to be 4.76 eV from the secondary electron energy threshold (see Fig. S6), in good agreement with the previously reported data (i.e., 4.7–4.8 eV) [37,38]. Likewise, the WFs of the K_4PTC and rGO-K_4PTC layers were determined as 4.03 and 3.99 eV, respectively. These values are lower than that measured for rGO (4.38 eV) or Al cathode (4.3 eV), displaying perfect match with the LUMO level of fullerene acceptor (3.91 eV) [29,30]. Since an ideal electron transport requires the LUMO level of the acceptor material being equal to the WF of the ETL [39], in the present work the energy level alignment at the active layer/ETL/Al interfaces may facilitate the electron transport from the fullerene acceptor to the ETL modified cathode (see Fig. 4a). Thus, these results trigger the use of K_4PTC and rGO-K_4PTC as an interlayer between the Al cathode and the active layer for efficient electron transport.

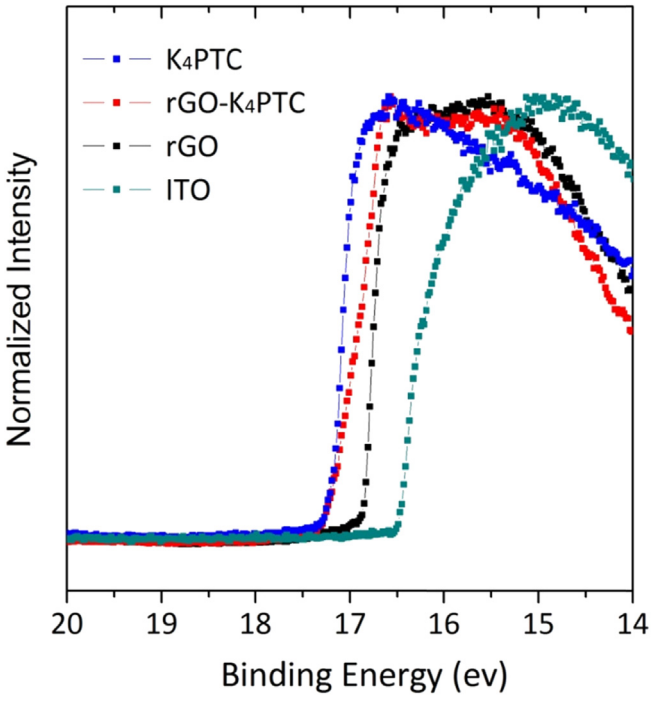

Fig. 3. UPS spectra of K_4PTC, rGO-K_4PTC and rGO films with ITO as substrate around the secondary-electron threshold region, in comparison with the bare ITO electrode.

3.2. Solar cells

To assess the electron transport capabilities of K_4PTC and rGO-K_4PTC, P3HT:PC_{61}BM-based PSCs with the respective ETLs were fabricated (see Fig. 4b). Fig. 5 shows their *J-V* curves, in comparison with those of reference devices. The averaged photovoltaic characteristics obtained from ten identical devices in each case are summarized in Table 1. The reference device with only the Al cathode showed a PCE of 2.24% with a J_{sc} of 7.25 mA cm^{-2}, a V_{oc} of 595 mV and a FF of 51.9%. Incorporation of K_4PTC or rGO-K_4PTC as an ETL between the active layer and the Al cathode increased the PCE by ca. 35%. In particular, the devices with the ETL yielded a PCE of 3.03/3.05%, with a J_{sc} of 8.37/8.52 mA cm^{-2}, a V_{oc} of 620/640 mV and a FF of 58.1/56.2%. Note that both the J_{sc} and FF are significantly improved as compared to those of the Al-only device, which may account for the major enhancement in PCE. As for the standard device with Ca/Al electrode, a PCE of 3.26% was obtained, only slightly higher than that of the device with K_4PTC or rGO-K_4PTC ETL. These results suggest that K_4PTC and rGO-K_4PTC can be utilized as efficient alternatives to the active Ca ETL for the P3HT:PC_{61}BM-based PSCs.

As shown in Table 1, the R_s of the device with ETL is remarkably lower than that of the Al-only device, in good agreement with their enhanced J_{sc}, FF and indicative of the electrical contribution from the ETL. On the other hand, the AFM technique was employed to study the surface morphologies of the P3HT:PC_{61}BM-based active layers with or without ETLs. The AFM height images are shown in Fig. S7. The RMS roughness of the bare active layer was determined as 12.7 nm, while the active layers with K_4PTC and rGO-K_4PTC ETLs exhibited the surfaces with smaller roughnesses of 6.5 nm and 9.2 nm, respectively. The smoother surface of the P3HT:PC_{61}BM/ETL system may facilitate the Al-coating, leading to better interfacial contact between the active layer and the cathode. These results also agree well with the reduced R_s in the devices with ETLs compared to that without ETL. In addition, IPCE measurements reveal that the device with K_4PTC or rGO-K_4PTC ETL yielded generally higher IPCE from 400 to 650 nm relative to that without ETL (see Fig. S8a), confirming the improved J_{sc} due to the incorporation of ETL.

To better understand the PCE increase in the PSC with ETL, we studied the electron mobilities in PSCs by using the space charge limited current (SCLC) technique [40,41]. Fig. 6 presents dark *J-V* curves of the devices with structure ITO/Cs_2CO_3/P3HT:PC_{61}BM/with or without ETL/Al. In particular, the data obtained in high-voltage region can be described using the Mott-Gurney equation: $J_{SCLC} = 9\varepsilon_0\varepsilon_\tau\mu_e(V\text{-}V_{BI})^2/(8\ L^3)$, where ε_0 is the free space permittivity, ε_τ is the dielectric constant of the material, V is the applied voltage, V_{BI} is the build-in voltage, L is the thickness of the active layer and

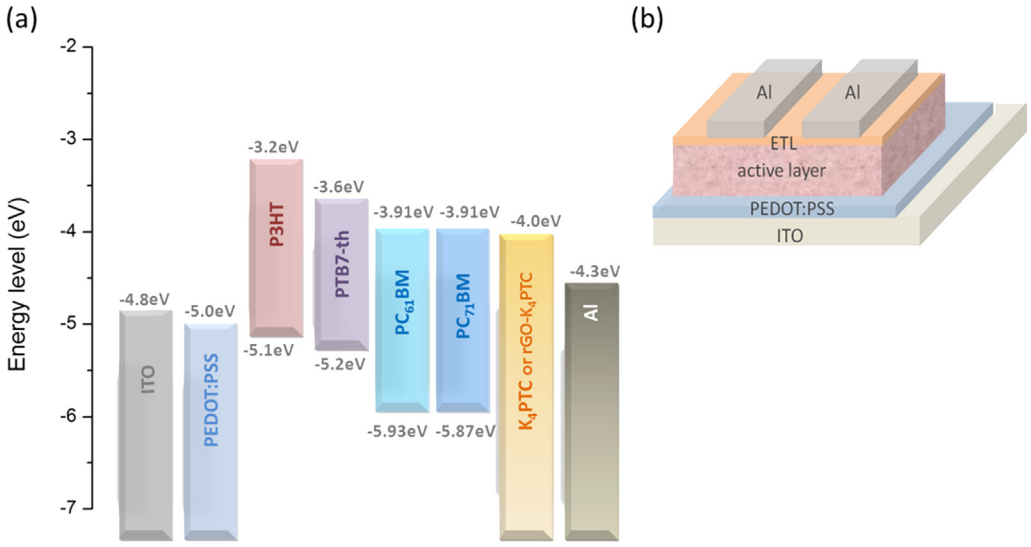

Fig. 4. (a) Energy level diagram for K_4PTC and rGO-K_4PTC determined from UPS and taken from the literature for other materials: P3HT, PTB7-th, PEDOT:PSS, $PC_{61}BM$, $PC_{71}BM$ and Al [27,29,30]. (b) Schematic structure of the PSC device with ETL.

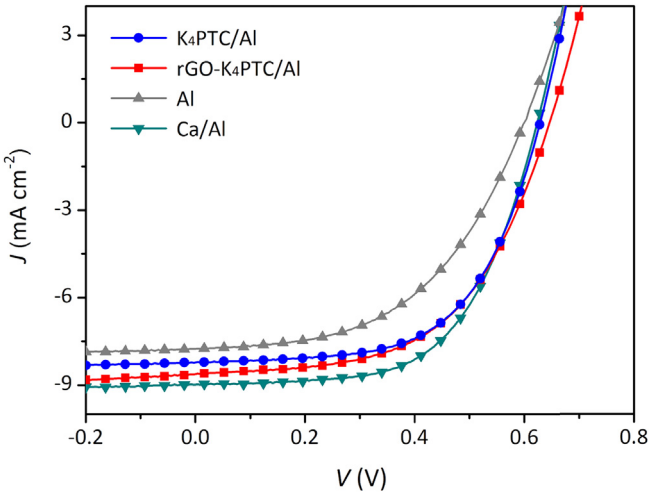

Fig. 5. *J–V* curves of the PSCs based on P3HT:$PC_{61}BM$ under the illumination of AM 1.5 G, 100 mW cm^{-2}.

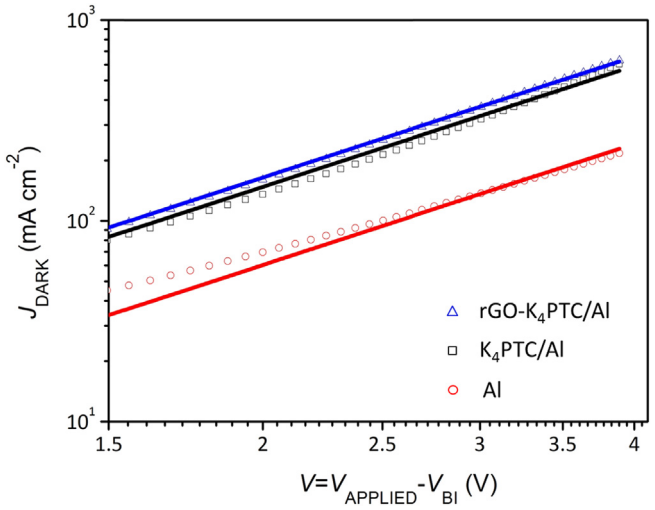

Fig. 6. *J-V* characteristics of the electron-only devices with or without ETL. The symbols represent experimental data, and the solid lines are obtained by fitting the experimental data with the SCLC model.

Table 1
Device performance[a] based on P3HT:$PC_{61}BM$ under 100 mW cm^{-2} AM 1.5G illumination with various ETLs.

ETL	J_{sc} (mA cm^{-2})	V_{oc} (mV)	FF (%)	PCE (%)[b]	R_s[c] (Ω cm^2)
w/o	7.25	595	51.9	2.24 (2.35)	21.8
K_4PTC	8.37	620	58.1	3.03 (3.07)	14.3
rGO-K_4PTC	8.52	640	56.2	3.05 (3.08)	16.9
Ca	8.58	628	60.5	3.26 (3.34)	14.0

[a] Averaged photovoltaic characteristics were obtained from 10 identical devices.
[b] The best PCE values are in brackets.
[c] Series resistance R_s was defined from the *J–V* curves of the best devices, using the method demonstrated in the literatures [21,22,28].

μ_e is the electron mobility. Accordingly, the electron mobilities in the devices with and without ETLs were calculated to be 9.52×10^{-4} cm^2V^{-1} s^{-1} (with K_4PTC ETL), 1.06×10^{-3} cm^2V^{-1} s^{-1} (with rGO-K_4PTC ETL) and 3.89×10^{-4} cm^2V^{-1} s^{-1}, respectively (see Supplementary file for calculation details). The higher electron mobility of the device with ETL might indicate better interfacial electron transfer between the active layer and the Al electrode. As a result, we rationally propose that the incorporation of ETL leads to an improved ohmic contact between the active layer and the Al cathode, and therefore gives rise to an enhanced PCE.

3.3. High-performance solar cells

To investigate the viability of K_4PTC and rGO-K_4PTC ETLs in high-performance PSCs, we applied them to PTB7-th:$PC_{61}BM$ devices, in which a low bandgap polymer PTB7-th was used as the electron donor. Table 2 summarizes the photovoltaic parameters of the PTB7-th:$PC_{61}BM$-based devices and their *J-V* curves are shown in Fig. 7. The incorporation of K_4PTC or rGO-K_4PTC as an interlayer between the active layer and the Al cathode significantly improved the PCE by ca. 28% as compared to that without ETL. In particular, the average PCE increases to 6.17/6.18% from 4.81% mainly due to the remarkably enhanced J_{sc} and FF. The best PCEs of 6.34% and 6.36% are slightly higher than that (6.05%) reported for the device

Table 2
Device performance[a] based on PTB7-th:$PC_{61}BM$ under 100 mW cm^{-2} AM 1.5G illumination with various ETLs.

ETL	J_{sc} (mA cm^{-2})	V_{oc} (mV)	FF (%)	PCE (%)[b]	R_s[c] (Ω cm^2)
w/o	10.66	771	58.8	4.82 (4.88)	11.6
K_4PTC	11.98	809	63.6	6.17 (6.34)	6.1
rGO-K_4PTC	12.34	808	62.0	6.18 (6.36)	6.2
Ca	12.63	802	64.2	6.50 (6.63)	6.5

[a] Averaged photovoltaic characteristics were obtained from 10 identical devices.
[b] The best PCE values are in brackets. Series resistance.
[c] Series resistance R_s was defined from the J–V curves of the best devices, using the method demonstrated in the literatures [21,22,28].

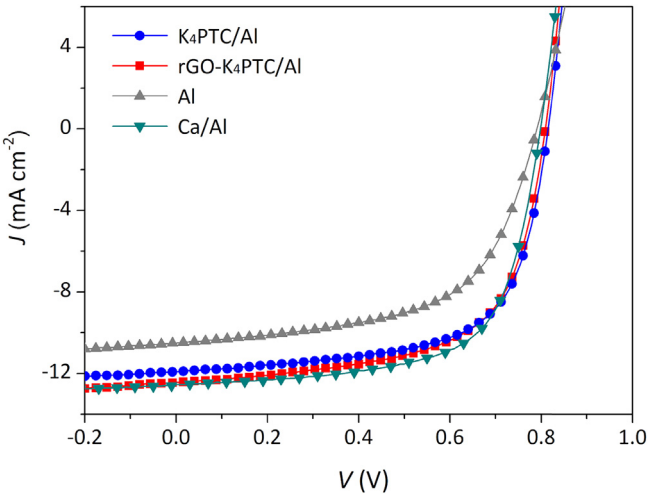

Fig. 7. J–V curves of the PSCs based on PTB7-th:$PC_{61}BM$, under the illumination of AM 1.5 G, 100 mW cm^{-2}.

with identical structure and a PDIN (a perylene diimide derivative with amino substituent) ETL [42], suggesting the superior electron transport capabilities of the K_4PTC and rGO-K_4PTC ETLs. Another reference device with Ca/Al cathode gave only slightly better average PCE of 6.55% with slightly higher J_{sc}, FF and comparable V_{oc}. The PTB7-th:$PC_{61}BM$-based devices with ETL also display higher IPCE plateau spectra from 350 to 750 nm in comparison with that without ETL (Fig. S8b), supporting the increase in J_{sc}.

In addition, K_4PTC and rGO-K_4PTC ETLs were also tested in another high-performance devices based on PTB7-th:$PC_{71}BM$. As listed in Table 3 and shown in Fig. 8, the device with K_4PTC or rGO-K_4PTC ETL gave an average PCE of 7.26%, with a J_{sc} of 14.19/14.59 mA cm^{-2}, a V_{oc} of 807/808 mV and FF of 63.4%/61.4%, which are all much better than those of the device without ETL (an average PCE of 5.52%, a J_{sc} of 12.05 mA cm^{-2}, a V_{oc} of 760 mV and FF of 60.3%) and fairly comparable to those of Ca/Al device (an average

Table 3
Device performance[a] based on PTB7-th:$PC_{71}BM$ under 100 mW cm^{-2} AM 1.5G illumination with various ETLs.

ETL	J_{sc} (mA cm^{-2})	V_{oc} (mV)	FF (%)	PCE (%)[b]	R_s[c] (Ω cm^2)
w/o	12.05	760	60.3	5.52 (5.62)	9.5
K_4PTC	14.19	807	63.4	7.26 (7.32)	5.6
rGO-K_4PTC	14.59	808	61.6	7.26 (7.30)	5.6
Ca	14.49	795	65.1	7.50 (7.60)	5.5

[a] Averaged photovoltaic characteristics were obtained from 5 identical devices.
[b] The best PCE values are in brackets. Series resistance
[c] Series resistance R_s was defined from the J–V curves of the best devices, using the method demonstrated in the literatures [21,22,28].

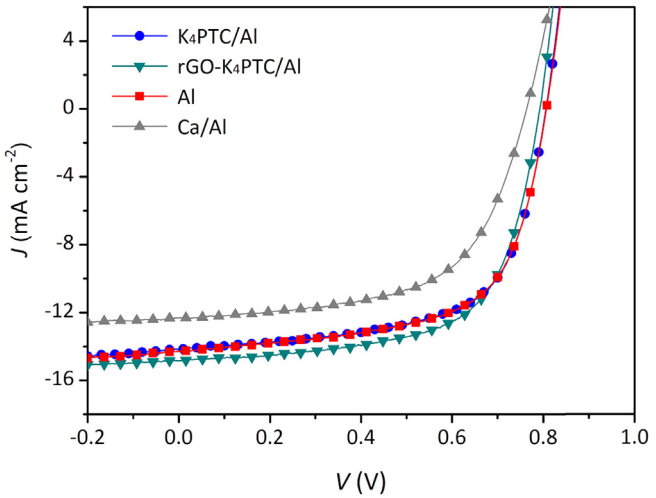

Fig. 8. J–V curves of the PSCs based on PTB7-th:$PC_{71}BM$, under the illumination of AM 1.5 G, 100 mW cm^{-2}.

PCE of 7.50%, a J_{sc} of 14.49 mA cm^{-2}, a V_{oc} of 795 mV and FF of 65.1%). Thus, these results confirm the possible use of K_4PTC and rGO-K_4PTC ETLs in PTB7-th-based devices.

3.4. Device stability

Since it has been reported that graphene showed resistance to oxygen and moisture [43,44], we thus expected that the incorporation of rGO-K_4PTC as the ETL would affect the device stability. To confirm this, degradation behaviors of the PSCs with ETL were studied under ca. 60% humidity without any encapsulation, which allows humidity directly affecting the device performance. Fig. 9 shows the PCE variation as a function of exposure time. The P3HT:$PC_{61}BM$-based device with rGO-K_4PTC ETL preserved 70% of the initial PCE in 8 h, almost comparable to that of the device with rGO as ETL (i.e., 65% of the initial PCE retained in 8 h, see Fig. S10). In comparison, the device with K_4PTC ETL showed a faster decay in PCE exhibiting only 27% PCE in 8 h, while the PCE of the Ca/Al declined sharply and dropped to 0 within 2 h. Thus, the tests demonstrate that utilizing rGO-K_4PTC as the ETL in P3HT:$PC_{61}BM$-

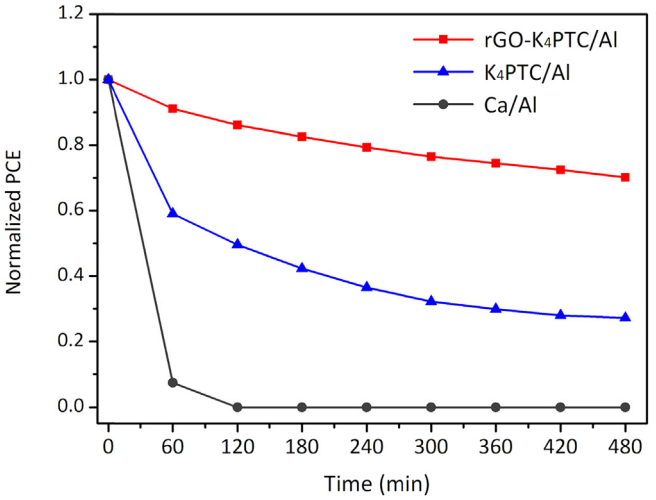

Fig. 9. Degradation of PCE with the exposure time for PSCs with various ETL materials and without encapsulation under ambient condition with relative humidity around 60%.

based PSC remarkably improved the device stability, which outperformed that with K_4PTC ETL. This result might indicate that rGO-K_4PTC can additionally act as an oxygen and moisture barrier, protecting the active layer against degradation.

4. Conclusions

In summary, we developed two solution-processable, air-stable, effective and inexpensive ETLs based on K_4PTC and rGO-K_4PTC, respectively. These ETLs have been applied to various PSCs that outperformed the reference devices without ETL, yielding increases of ~35% in PCEs. Particularly, the P3HT:PC_{61}BM based PSCs with respective ETL showed an average PCE of 3.03–3.05%, while the PTB7-th:PC_{61}BM and PTB7-th:PC_{71}BM-based PSCs gave average PCEs of 6.17–6.18% and 7.26%, respectively. These PCE values are even fairly comparable to those obtained from standard Ca/Al devices, indicating good electron extraction or transport capabilities of K_4PTC and rGO-K_4PTC-based interlayers. These have been attributed principally to the low WFs of K_4PTC and rGO-K_4PTC (4.0 eV), which perfectly matches the LUMO level of fullerene acceptor, ensuring an improved ohmic contact at the acceptor-cathode interface. Furthermore, we demonstrated that rGO-K_4PTC-based ETL could additionally serve as a shielding layer against the oxygen and humidity, protecting the active layer and leading to better device stability in air. We thus anticipate that the rGO-K_4PTC-based ETL is more suitable for real applications relative to the K_4PTC-based ETL.

Acknowledgments

This work is the supported in part by the Natural Science Foundation of China (51372158), Jiangsu Specially Appointed Professor Program (SR10800113), the Project for Jiangsu Scientific and Technological Innovation Team (2013), Ministry of Education of China, and a Project Funded by the Priority Academic Program Development of Jiangsu Higher Education Institutions (PAPD).

Appendix A. Supplementary data

Supplementary data related to this article can be found at http://dx.doi.org/10.1016/j.orgel.2016.06.013.

References

[1] S. Günes, H. Neugebauer, N.S. Sariciftci, Conjugated polymer-based organic solar cells, Chem. Rev. 107 (2007) 1324–1338.
[2] B.C. Thompson, M.J. Fréchet, Polymer–fullerene composite solar cells, Angew. Chem. Int. Ed. 47 (2008) 58–77.
[3] G. Dennler, M.C. Scharber, C.J. Brabec, Polymer-fullerene bulk-heterojunction solar cells, Adv. Mater. 21 (2009) 1323–1338.
[4] L. Lu, T. Zheng, Q. Wu, A.M. Schneider, D. Zhao, L. Yu, Recent advances in bulk heterojunction polymer solar cells, Chem. Rev. 115 (2015) 12666–12731.
[5] J. You, L. Dou, K. Yoshimura, T. Kato, K. Ohya, T. Moriarty, K. Emery, C.-C. Chen, J. Gao, G. Li, Y. Yang, A polymer tandem solar cell with 10.6% power conversion efficiency, Nat. Commun. 4 (2013) 1446.
[6] H. Zhou, Y. Zhang, C.-K. Mai, S.D. Collins, G.C. Bazan, T.Q. Nguyen, A.J. Heeger, Polymer homo-tandem solar cells with best efficiency of 11.3%, Adv. Mater. 27 (2015) 1767–1773.
[7] J.D. Chen, C. Cui, Y.Q. Li, L. Zhou, Q.D. Ou, C. Li, Y.F. Li, J.X. Tang, Single-junction polymer solar cells exceeding 10% power conversion efficiency, Adv. Mater. 27 (2015) 1035–1041.
[8] J.U. Lee, J.W. Jung, J.W. Jo, W.H. Jo, Degradation and stability of polymer-based solar cells, J. Mater. Chem. 22 (2012) 24265–24283.
[9] M. Jørgensen, K. Norrman, S. Gevorgyan, T. Tromholt, B. Andreasen, F. Krebs, Stability of polymer solar cells, Adv. Mater. 24 (2012) 580–612.
[10] G. Williams, Q. Wang, H. Aziz, The photo-stability of polymer solar cells: contact photo-degradation and the benefits of interfacial layers, Adv. Funct. Mater. 23 (2013) 2239–2247.
[11] M.O. Reese, A.J. Morfa, M.S. White, N. Kopidakis, S.E. Shaheen, G. Rumbles, D.S. Ginley, Pathways for the degradation of organic photovoltaic P3HT: PCBM based devices, Sol. Energy Mater. Sol. Cells 92 (2008) 746–752.
[12] M.O. Reese, M.S. White, G. Rumbles, D.S. Ginley, S.E. Shaheen, Optimal negative electrodes for poly(3-hexylthiophene): [6,6]-Phenyl C_{61}-Butyric acid methyl ester bulk heterojunction photovoltaic devices, Appl. Phys. Lett. 92 (2008) 053307.
[13] N. Sekine, C.-H. Chou, W.L. Kwan, Y. Yang, ZnO nano-ridge structure and its application in inverted polymer solar cell, Org. Electron. 10 (2009) 1473–1477.
[14] H.-L. Yip, S.K. Hau, N.S. Baek, H. Ma, A.K.-Y. Jen, Polymer solar cells that use self-assembled-monolayer-modified ZnO/metals as cathodes, Adv. Mater. 20 (2008) 2376–2382.
[15] J.Y. Kim, S.H. Kim, H.H. Lee, K. Lee, W. Ma, X. Gong, A.J. Heeger, New architecture for high-efficiency polymer photovoltaic cells using solution-based titanium oxide as an optical spacer, Adv. Mater. 18 (2006) 572–576.
[16] C. Tao, S.P. Ruan, X.D. Zhang, G.H. Xie, L. Shen, X.Z. Kong, W. Dong, C.X. Liu, W.Y. Chen, Performance improvement of inverted polymer solar cells with different top electrodes by introducing a MoO_3 buffer layer, Appl. Phys. Lett. 93 (2008) 193307.
[17] S.J. Yoon, J.H. Park, H.K. Lee, O.O. Park, Low vacuum process for polymer solar cells: effect of $TiO_{(x)}$ interlayer, Appl. Phys. Lett. 92 (2008) 143504.
[18] S.-H. Liao, Y.-L. Li, T.-H. Jen, Y.-S. Cheng, S.-A. Chen, Multiple functionalities of polyfluorene grafted with metal ion-intercalated crown ether as an electron transport layer for bulk-heterojunction polymer solar cells: optical interference, hole blocking, interfacial dipole, and electron conduction, J. Am. Chem. Soc. 134 (2012) 14271–14274.
[19] C.-H. Wu, C.-Y. Chin, T.-Y. Chen, S.-N. Hsieh, C.-H. Lee, T.-F. Guo, A.K.-Y. Jen, T.-C. Wen, Enhanced performance of polymer solar cells using solution-processed tetra-N-alkyl ammonium bromides as eelectron extraction layers, J. Mater. Chem. A 1 (2013) 2582–2587.
[20] L. Hu, F. Wu, C. Li, A. Hu, X. Hu, Y. Zhang, L. Chen, Y. Chen, Alcohol-soluble n-type conjugated polyelectrolyte as electron transport layer for polymer solar cells, Macromolecules 48 (2015) 5578–5586.
[21] Z.G. Zhang, B.Y. Qi, Z.W. Jin, D. Chi, Z. Qi, Y.F. Li, J.Z. Wang, Perylene diimides: a thickness-insensitive cathode interlayer for high performance polymer solar cells, Energy Environ. Sci. 7 (2014) 1966–1973.
[22] X.D. Liu, W.-X. Jiao, M. Lei, Y. Zhou, B. Song, Y.F. Li, Crown-ether functionalized fullerene as a solution processable cathode buffer layer for high performance perovskite and polymer solar cells, J. Mater. Chem. A 3 (2015) 9278–9284.
[23] C.-Y. Chang, W.-K. Huang, Y.-C. Chang, K.-T. Lee, H.-Y. Siao, High-performance flexible tandem polymer solar cell employing a novel cross-linked conductive fullerene as an electron transport layer, Chem. Mater. 27 (2015) 1869–1875.
[24] C. Yi, K. Yue, W.B. Zhang, X.-C. Lu, J.H. Hou, Y.F. Li, L. Huang, G.R. Newkome, S.Z.D. Cheng, X. Gong, Conductive water/alcohol-soluble neutral fullerene derivative as an interfacial layer for inverted polymer solar cells with high efficiency, ACS Appl. Mater. Interfaces 6 (2014) 14189–14195.
[25] Q. Mei, C.-H. Li, X. Gong, H. Lu, E.Q. Jin, C. Du, Z. Lu, L. Jiang, X. Meng, C. Wang, Z. Bo, Enhancing the performance of polymer photovoltaic cells by using an alcohol soluble fullerene derivatives as the interfacial layer, ACS Appl. Mater. Interfaces 5 (2013) 8076–8080.
[26] J. Liu, M. Durstock, L.-M. Dai, Graphene oxide derivatives as hole- and electron extraction layers for high-performance polymer solar cells, Energy Environ. Sci. 7 (2014) 1297–1306.
[27] S.-X. Qu, M.-H. Li, L.-X. Xie, X. Huang, J.-G. Yang, N. Wang, S. Yang, Non-covalent functionalization of graphene attaching [6,6]-Phenyl-C61-Butyric acid methyl ester (PCBM) and application as electron extraction layer of polymer solar cells, ACS Nano. 7 (2013) 4070–4081.
[28] G. Kakavelakis, D. Konios, E. Stratakis, E. Kymakis, Enhancement of the efficiency and stability of organic photovoltaic devices via the addition of a lithium-neutralized graphene oxide electron-transporting layer, Chem. Mater. 26 (2014) 5988–5993.
[29] J. Liu, Y.-H. Xue, Y.-X. Gao, D.-S. Yu, M. Durstock, L.-M. Dai, Hole and electron extraction layers based on graphene oxide derivatives for high-performance bulk heterojunction solar cells, Adv. Mater. 24 (2012) 2228–2233.
[30] Y. He, Y. Li, Fullerene derivative acceptors for high performance polymer solar cells, Phys. Chem. Chem. Phys. 13 (2011) 1970–1983.
[31] S.-H. Liao, H.-J. Jhuo, Y.-S. Cheng, S.-A. Chen, Fullerene derivative-doped zinc oxide nanofilm as the cathode of inverted polymer solar cells with low-bandgap polymer (PTB7-Th) for high performance, Adv. Mater. 25 (2013) 4766–4771.
[32] M. Majumder, P. Sheath, J.I. Mardel, T.G. Harvey, A.W. Thornton, A. Gonzago, et al., Aqueous molecular sieving and strong gas adsorption in highly porous MOFs with a facile synthesis, Chem. Mater. 24 (2012) 4647–4652.
[33] D. Li, M.B. Müller, S. Gilje, R.B. Kaner, G.G. Wallace, Processable aqueous dispersions of graphene nanosheets, Nat. Nanotechnol. 3 (2008) 101–105.
[34] S.K. Gupta, S. Setia, S. Sidiq, M. Gupta, S. Kumar, S.K. Pal, New perylene-based non-conventional discotic liquid crystals, RSC Adv. 3 (2013) 12060–12065.
[35] X. Wang, M. Tabakman, S.H. Dai, Atomic layer deposition of metal oxides on pristine and functionalized graphene, J. Am. Chem. Soc. 130 (2008) 8152–8153.
[36] C. Deng, W. Lin, G. Agnus, D. Dragoe, D. Pierucci, A. Ouerghi, S. Eimer, I. Barisic, D. Ravelosona, C. Chappert, W. Zhao, Reversible charge-transfer doping in graphene due to reaction with polymer residues, J. Phys. Chem. C 118 (2014) 13890–13897.
[37] X.-A. Cao, Y.-Q. Zhang, Performance enhancement of organic light-emitting diodes by chlorine plasma treatment of indium tin oxide, Appl. Phys. Lett. 100 (2012) 183304.

[38] M.G. Helander, Z.-B. Wang, J. Qiu, M.T. Greiner, D.P. Puzzo, Z.-W. Liu, Z.H. Lu, Chlorinated indium tin oxide electrodes with high work function for organic device compatibility, Science 332 (2011) 944–947.
[39] C.-C. Chueh, C.-Z. Li, A.K.-Y. Jen, Recent progress and perspective in solution-processed interfacial materials for efficient and stable polymer and organo-metal perovskite solar cells, Energy Environ. Sci. 8 (2015) 1160–1189.
[40] P.W.M. Blom, C. Tanase, D.M. de Leeuw, R. Coehoorn, Thickness scaling of the space-charge-limited current in poly(p-phenylenevinylene), Appl. Phys. Lett. 86 (2005) 092105.
[41] Z.-S. An, J.-S. Yu, S.C. Jones, S. Barlow, S. Yoo, B. Domercq, P. Prins, L. D. A. Siebbeles, B. Kippelen, S.R. Marder, High electron mobility in room-temperature discotic liquid- crystalline perylene diimides, Adv. Mater. 17 (2005) 2580–2583.
[42] Y. Lin, J. Wang, Z.-G. Zhang, H. Bai, Y. Li, D. Zhu, X. Zhan, An electron acceptor challenging fullerenes for efficient polymer solar cells, Adv. Mater. 27 (2015) 1170–1174.
[43] J.-S. Wu, W. Pisula, K. Müllen, Graphenes: potential material for electronics, Chem. Rev. 107 (2007) 718–747.
[44] M.F. Chisholm, G. Duscher, W. Windl, Oxidation resistance of reactive atoms in graphene, Nano Lett. 12 (2012) 4651–4655.